J Biol Inorg Chem (2011) 16:1227–1239
DOI 10.1007/s00775-011-0811-x

ORIGINAL PAPER

# A novel insight into the heme and NO/CO binding mechanism of the alpha subunit of human soluble guanylate cyclase

**Fangfang Zhong · Jie Pan · Xiaoxiao Liu · Hongyan Wang · Tianlei Ying · Jihu Su · Zhong-Xian Huang · Xiangshi Tan**

Received: 22 February 2011 / Accepted: 20 June 2011 / Published online: 2 July 2011


**Abstract** Human soluble guanylate cyclase (sGC), a critical heme-containing enzyme in the NO-signaling pathway of eukaryotes, is an $\alpha\beta$ heterodimeric hemoprotein. Upon the binding of NO to the heme, sGC catalyzes the conversion of GTP to cyclic GMP, playing a crucial role in many physiological processes. However, the specific contribution of the $\alpha$ and $\beta$ subunits of sGC in the intact heme binding remained intangible. The recombinant human sGC $\alpha$1 subunit has been expressed in *Escherichia coli* and characterized for the first time. The heme binding and related NO/CO binding properties of both the $\alpha$1 subunit and the $\beta$1 subunit were investigated via heme reconstitution, UV–vis spectroscopy, EPR spectroscopy, stopped-flow kinetics, and homology modeling. These results indicated that the $\alpha$1 subunit of human sGC, lacking the conserved axial ligand, is likely to interact with heme noncovalently. On the basis of the equilibrium and kinetics of CO binding to sGC, one possible CO binding model was proposed. CO binds to human sGC$\beta$195 by simple one-step binding, whereas CO binds to human sGC$\alpha$259, possibly from both axial positions through a more complex process. The kinetics of NO dissociation from human sGC indicated that the NO dissociation from sGC was complex, with at least two release phases, and human sGC$\alpha$259 has a smaller $k_1$ but a larger $k_2$. Additionally, the role of the cavity of the $\alpha$1 subunit of human sGC was explored, and the results indicate that the cavity likely accommodates heme. These results are beneficial for understanding the overall structure of the heme binding site of the human sGC and the NO/CO signaling mechanism.

**Keywords** Human soluble guanylate cyclase · NO/CO binding · Heme binding · NO/CO signaling · YC-1

**Abbreviations**

| | |
|---|---|
| cDNA | Complementary DNA |
| cGMP | Guanosine 3′,5′-cyclic monophosphate |
| DEA/NO | Diethylammonium (*Z*)-1-(*N*,*N*-diethylamino)-diazen-1-ium-1,2-diolate |
| DTT | Dithiothreitol |
| H-NOX domain | Heme–nitric oxide/oxygen binding domain |
| hsGC | Human soluble guanylate cyclase |
| hsGC$\alpha$259 | N-terminus truncated human soluble guanylate cyclase $\alpha$1 subunit with residues 65–259 |
| hsGC$\alpha$385 | N-terminus truncated human soluble guanylate cyclase $\alpha$1 subunit with residues 65–385 |
| hsGC$\alpha$690 | Full-length human soluble guanylate cyclase $\alpha$1 subunit with residues 1–690 |
| sGC | Soluble guanylate cyclase |
| YC-1 | 5-[1-(Phenylmethyl)-1*H*-indazol-3-yl]-2-furanmethanol |

F. Zhong · J. Pan · X. Liu · T. Ying · Z.-X. Huang · X. Tan (✉)
Department of Chemistry,
Fudan University,
Shanghai 200433, China
e-mail: xstan@fudan.edu.cn

H. Wang · X. Tan
Institutes of Biomedical Sciences,
Fudan University,
Shanghai 200433, China

J. Su
Department of Modern Physics,
University of Science and Technology of China,
Hefei 230026, China

## Introduction

Nitric oxide, as a signaling molecule in the cardiovascular system, plays an important role in several vital physiological processes. The primary NO receptor is soluble guanylate cyclase (sGC), a crucial heme-containing enzyme in the NO-signaling pathway of eukaryotes. Upon NO binding, sGC catalyzes the conversion of the substrate guanosine 5′-triphosphate to 3′,5′-cyclic guanosine monophosphate (cGMP), which initiates the NO-dependent signaling cascades. cGMP, an important second messenger, regulates various effector proteins and plays a critical role in many physiological processes, such as blood pressure, vasodilatation, platelet aggregation, tissue development, and neuronal transmission [1–4]. Dysfunction of NO signaling results in several pathological disorders, ranging from many cardiovascular diseases, such as arterial hypertension, pulmonary hypertension, heart failure, atherosclerosis, and restenosis, to neurodegenerative diseases [3].

sGC in eukaryotes is a heterodimeric hemoprotein, composed of $\alpha$ and $\beta$ subunits with the $\alpha1\beta1$ heterodimer as the abundant form. The prosthetic heme moiety, crucial for NO/CO sensing and regulation, is located in the heme-binding domain of sGC through proximal $\beta1$ His105 [3, 5, 6]. Apart from the axial ligand, the overall structure of the heme environment in sGC is essential for the physiological function [7, 8]. However, it is still unclear how the two subunits contribute to the intact heme binding of sGC. The heme content is routinely determined with the pyridine hemochromogen method and Bradford's protein assay; however, since the heterodimeric sGC easily loses heme upon purification, it is controversial whether the native heme stoichiometry is one or two per heterodimer according to different purification methods [7, 9, 10]. It has been hypothesized that the heme is sandwiched between the $\alpha1$ and $\beta1$ subunits of sGC; however, there is no direct evidence that only the $\beta1$ subunit can bind heme. There is a large cavity in the $\alpha1$ subunit homology model of sGC based on the considerable sequence homology between the $\alpha1$ and $\beta1$ subunits [11], and furthermore, it was suggested by several mutagenic studies that the N-terminus of the $\alpha1$ subunit contributed to heme loading in sGC [8, 12], indicating that heme could be accommodated in the cavity similar to that in the case of the $\beta1$ subunit.

Previously, heme and NO/CO binding features of sGC were extensively studied [7, 12–16]. However, nearly all of the studies were based on the heterodimeric sGC or only the $\beta1$ subunit; therefore, the heme and NO/CO binding properties of the $\alpha1$ subunit remained undiscovered. If the $\alpha1$ subunit can indeed contribute to heme binding, it will be essential to understand the $\alpha1$-subunit-related heme and NO/CO binding mechanism to understand the mechanism of sGC-mediated NO signaling.

5-[1-(Phenylmethyl)-1*H*-indazol-3-yl]-2-furanmethanol (YC-1), a benzylindazole derivative with antiplatelet activity, can potentiate the activation of sGC upon CO binding [3, 17]. However, the location of the YC-1 binding site of sGC is still ambiguous. Several possible sites were suggested, including the pocket of the $\beta1$ subunit or the $\alpha1$ subunit, and the allosteric site near the heme pocket or the catalytic domain (interaction with $\alpha1$Cys596 and $\beta1$Cys541) [12, 18–21]. Recently, YC-1 was proposed to occupy the cavity of the sGC $\alpha1$ subunit and the docking model was described [11]; however, there is no direct evidence to verify the hypothesis. The mechanism of the synergistic activation of YC-1 is also a matter of debate, one possible mechanism is involved in reducing the CO dissociation rate and further increasing the CO affinity [12, 22, 23].

To explore the mechanism of sGC-mediated NO singling, we established an efficient expression system of human sGC (hsGC) in *Escherichia coli* to obtain pure hsGC protein in large quantities [13], resolving the bottle-neck problem for this study. Herein, we report, for the first time, the preparation and characterization of recombinant hsGC $\alpha1$ subunit in full-length form (hsGC$\alpha$690) and its truncated N-terminal fragments (hsGC$\alpha$259 and hsGC$\alpha$385). The heme and NO/CO binding mechanism of the $\alpha1$ subunit of sGC was addressed and investigated with the heme domain via heme reconstitution, UV–vis and EPR spectroscopy, stopped-flow kinetics, and the homology modeling. Furthermore, we evaluated the possibility of YC-1 occupying the cavity of the sGC $\alpha1$ subunit by isothermal titration calorimetry and examined the effect of YC-1 on CO binding affinity.

## Materials and methods

### Materials

Plasmid FL13315 containing the entire hsGC $\alpha1$ complementary DNA (cDNA) was purchased from Fulengen, China. The MBPHT-mCherry2 vector was a kind gift from Yu Ding (School of Life Sciences, Fudan University). hsGC$\beta$195 (N-terminus truncated human soluble guanylate cyclase $\beta1$ subunit with residues 1-195) was expressed and purified as described previously [13]. The TEV protease expression vector pRK1043 and the *E. coli* strains XL10-Gold, Rosetta (DE3) pLysS, and BL21-Condon Plus were obtained from Novagen. Pfu DNA polymerase, T4 DNA ligase, dNTP, and restriction enzymes (*Bam*HI, *Hin*dIII, *Eco*RI, and *Xho*I) were purchased from New England Biolabs. Oligonucleotide PCR primer pairs, labeled as P1, P2, and P3, were synthesized and DNA sequencing reactions were performed by Shanghai Invitrogen Biotech. The primer pairs were as follows:

P1: [5′-TGAATTCGAAAACCTGTATTTTCAGGGTG GTGGTGGTAGTCGGAGCCGAG-3′(F); 5′-CCTCTCG AGTTAGTGATGGTGATGGTGATGCATGTGAACGG AG-3′(R)]

P2: [5′-ATGGATCCGGCGGCAGCGGTAGTCGGAG CCGAGTCTATC-3′(F); 5′-CCCAAGCTTTCAGGGTGA CCCCAAAAACAAG-3′(R)]

P3: [5′-ATGGATCCGGCAGCGGTATGTTCTGCAC GAAGC-3′(F); 5′-CCCAAGCTTTCAATCTATTCCTGA TGCTTTGC-3′(R)]

The plasmid purification kits, gel extraction kits, nickel nitrilotriacetic acid resin, and Sephadex G-25 resin were purchased from QIAGEN (Chatsworth, CA, USA). The Superdex$^{TM}$ 200 HiLoad 16/60 gel filtration column was from Pharmacia. Hemin and sperm whale myoglobin were from Sigma. YC-1 and diethylammonium (Z)-1-(*N*,*N*-diethylamino)-diazen-1-ium-1,2-diolate (DEA/NO) were purchased from Cayman Chemical Company. Carbon monoxide was from Matheson. All other reagents were of analytic grade.

## Cloning, expression, and purification of hsGCα259, hsGCα385, and hsGCα690

hsGCα259, hsGCα385, and hsGCα690 (encoding hsGC α1 N-terminal fragment cDNA residues 65–259, 65–385, and 1–690, respectively) were amplified using plasmid FL13315 containing the entire hsGC α1 cDNA as a template. PCR products were obtained using the primer pairs P1, P2, and P3 for hsGCα259, hsGCα385 and hsGCα690, respectively. The PCR products were digested and ligated into MBPHT-mCherry2 vector, and the constructed plasmid was verified by DNA sequencing. The verified plasmids were transformed into Rosetta (DE3) pLysS or BL21-Condon Plus competent cells for expression. The expression and purification of hsGCα259, hsGCα385, and hsGCα690 were performed according to a previously published protocol [13]. The purified apoprotein in buffer A [50 mM tris(hydroxymethyl)aminomethane hydrochloride, 100 mM NaCl, pH 7.4] was collected, concentrated, and stored at −80 °C. The purity of proteins obtained was assessed by imaging 15% sodium dodecyl sulfate–polyacrylamide gel electrophoresis gel stained with Coomassie Blue.

## Heme reconstitution

The hsGCα259 was isolated with a little amount of heme. To identify the heme binding properties of hsGCα259, heme reconstitution was conducted as described previously [13]. Apo-hsGCα259 in buffer A containing 5 mM dithiothreitol (DTT) was used for reconstitution with heme by adding 5 equiv of hemin stock solution freshly prepared at 4 °C overnight; the unbound hemin was then removed by Sephadex G-25. The elution fractions from the Sephadex G-25 column, identified by a characteristic deep red-brown color and the UV–vis spectrum, were pooled and concentrated, and then subjected to the Superdex$^{TM}$ 200 HiLoad 16/60 gel filtration column equilibrated with buffer A. Fractions containing hsGCα259 were collected, concentrated, frozen in liquid nitrogen, and stored at −80 °C. The protein concentration was determined by the Bradford method, and the heme concentration in the protein samples was measured by the pyridine–hemochromogen assay with an extinction coefficient of $\varepsilon_{R\text{-}O,557-540} = 22.1$ $mM^{-1}$ $cm^{-1}$ [24]. The heme reconstitution of hsGCα385 and hsGCα690 was performed with the same procedure as described above.

## Molecular modeling of N-terminal hsGC α1

The sequence of the α1 subunit of hsGC was submitted to the Robetta structure prediction server for domain prediction [25]. The 60 N-terminal residues were predicted to be disordered and the following 200 residues were predicted to belong to a heme-nitric oxide/oxygen binding domain (H-NOX domain), which shares strong sequence homology with mammalian sGC [26]. The molecular modeling procedure was performed as described in [13]. The initial coordinates for hsGCα259 were constructed on the basis of the crystal structure of the H-NOX domain of *Nostoc* sp. (Protein Data Bank entry 2O09) [27] via homology modeling (http://swissmodel.expasy.org/SWISS-MODEL.html). Water molecules in the crystal structure were retained in the simulation. Force field parameters for heme were adopted from previously publications [28, 29] and the peptide was simulated with the CHARMM force field [30]. The structure was first minimized for 1,000 steps with the conjugate gradient method, was equilibrated for 10 ps with a time step of 1 fs, and then was further minimized for 180,000 steps. The NAMD program was used for simulations, and the VMD program was employed for structural analysis.

## UV–vis spectroscopy

Electronic absorption spectra of hsGCα259 in buffer B (50 mM potassium phosphate, pH 7.4, 100 mM KCl, 5% glycerol), were recorded with an HP8453 UV–vis spectrophotometer. The protein concentration was about 3 μM. The protein sample was prepared in a glove box (MBraun) under a highly pure $N_2$ atmosphere and transferred into an anaerobic cuvette. The ferrous protein was obtained by adding 10 mM dithionite or 100 μM titanium(III) citrate. NO was generated by the reaction of $NaNO_2$ and HCl, and was passed through an aqueous solution of sodium hydroxide to eliminate possible contamination of acid and

higher oxides of nitrogen. The NO/CO-bound protein complex was then produced by bubbling with NO/CO for 5 min. YC-1 (50 μM) was added to the CO-bound hsGC protein sample and the mixture was incubated for 10 min before the addition of CO at 20 °C to check the effect of YC-1 on CO binding affinity.

### EPR spectroscopy

The X-band EPR of hsGCα259 and that of hsGCβ195 in the ferric state were recorded at −266 °C with a Bruker Elexsys E580 spectrometer equipped with an EN 4118X-MD4 pulsed electron–nuclear double resonance resonator and an Oxford Instruments ESR900 liquid-helium cryostat and an ITC503 temperature controller. The EPR conditions were microwave frequency 9.72 GHz and microwave power 0.2 mW.

NO-bound hsGCα259 was prepared anaerobically in the glove box under a highly pure $N_2$ atmosphere using the same procedure as for hsGCβ195 [13]. X-band EPR spectra were recorded at −173 °C with a Bruker BioSpin spectrometer. The spectra were recorded under the following conditions: microwave frequency 9.44 GHz, microwave power 2.0 mW, modulation frequency 100 kHz, modulation amplitude 4.00 G, and time constant 163.84 ms. The concentrations of the NO-bound samples were about 120 and 60 μM, respectively.

### Interaction of heme with apo-hsGC

Heme dissociation rate constants ($k_{off}$) were measured by stopped-flow apparatus or a UV–vis spectrometer with kinetic mode in heme transfer experiments using the apomyoglobin assay [31, 32]. Pre-steady-state stopped-flow experiments were performed at 25 °C with an SF-61 DX2 double-mixing stopped-flow instrument (Hi-Tech, UK) installed in a glove box (MBraun, MB100 with an $O_2$ analyzer to ensure that the $O_2$ concentration was below 1 ppm) [31, 32]. The heme transfer reactions were initiated by mixing 1.5 μM reconstituted hsGCα259 or hsGCβ195 with 10 μM apomyoglobin and were monitored as the increase in absorbance at 409 nm. CO–heme was produced by bubbling CO into the hemin solution for 10 min and the concentration was then determined using $\varepsilon_{407} = 147\ mM^{-1}\ cm^{-1}$ [32]. CO–heme does exist as a monomer at concentrations below 5–10 μM; therefore, the binding of CO and heme is assumed to apply to monomeric heme binding [31–33]. The heme association rate constants ($k_{on}$) were measured by mixing 2 μM CO–heme in buffer C (50 mM potassium phosphate, pH 7.4, 100 mM KCl, 5% glycerol, 2 mM DTT, 30 mM $Na_2S_2O_4$) with 1 μM apo-hsGC prepared in a highly pure $N_2$ atmosphere glove box at room temperature (20 °C). The reactions of apo-hsGCα259 or apo-hsGCβ195 with CO–heme were monitored at 420 nm. Apomyoglobin was prepared using the methyl ethyl ketone extraction method as described in [34].

### Kinetics of NO/CO binding and dissociation of hsGC

#### *CO dissociation equilibrium*

CO titration experiments were performed as previously described with some modifications [12]. The hsGC protein sample was prepared in a septum-capped cuvette in buffer C with minimal head space in a highly pure $N_2$ atmosphere glove box at room temperature (20 °C). Aliquots of CO-saturated buffer C, assumed to be 1 mM in CO, were added to the cuvette via a syringe and were equilibrated for 2 min, and the spectra were recorded. The dilution induced by the addition of CO was considered and the spectra were corrected by absorbance times the dilution factor. The change in the spectra was estimated as $A_{416}$–$A_{434}$ and $A_{420}$–$A_{437}$ for hsGCα259 and hsGCβ195, respectively. Data were fitted to a single-site saturation ligand binding model using Sigma Plot (SPSS, Chicago, IL, USA).

#### *Kinetics of CO binding and release*

The kinetics of the CO binding process was measured for a series of CO concentrations (0.01–0.5 mM) with a stopped-flow instrument by monitoring the absorbance change ($A_{416}$–$A_{434}$, $A_{420}$–$A_{437}$ for hsGCα259 and hsGCβ195. The reaction time courses were analyzed by nonlinear regression to single- or double-exponential functions, from which the observed rate constants ($k_{obs}$) were obtained. The $k_{on}$ and $k_{off}$ values were obtained from the slope and intercept, respectively, in plots of $k_{obs}$ against CO concentration. $k_{off}$ divided by $k_{on}$ gave the calculated value for $K_d$ of the binding process.

#### *Kinetics of NO dissociation from hsGC*

Dissociation of NO from the heme of hsGC was estimated at 20 °C using the CO/dithionite trapping method, as described previously [23, 35]. The proteins were prepared in buffer D (50 mM potassium phosphate, pH 7.4, 100 mM KCl, 5% glycerol, 2 mM DTT) and were reduced by 100 μM titanium(III) citrate in a highly pure $N_2$ atmosphere glove box. NO (10 μM), released from DEA/NO, was added to the protein sample, and the spectrum was recorded to identify the formation of NO-bound sGC. The CO/dithionite trapping solution was prepared by bubbling CO into a freshly prepared dithionite solution. The reaction was initiated by the addition of CO/dithionite solution to the protein sample via a syringe, and was measured by electronic absorption spectroscopy using an HP8453

UV–vis spectrophotometer with kinetic mode at 20 °C. The final concentrations of $Na_2S_2O_4$ and protein were 30 mM and 2 μM, respectively. The spectra were recorded every 10 s for the first 10 min, every 1 min for the next 1 h, and every 2 min thereafter for a total of 3 h, or until the reaction reached equilibrium.

### Isothermal titration calorimetry

Titrations were performed at 25 °C using a MicroCal iTC200 titration calorimeter. Apo-hsGCα259 protein and YC-1 were suspended in buffer E [50 mM 4-(2-hydroxyethyl)-1-piperazineethane sulfonic acid, pH 7.4, 1 mM tris(2-carboxyethyl)phosphine, 100 mM NaCl]. All the solutions were degassed by centrifuging them for 5 min before use. The titration involved 252-μl injections of 1 mM YC-1 into 20–100 μM apo-hsGCα259 contained in the cell (cell volume 200 μl), with intervals of 2 min between injections. Curve fitting was performed using the Omega.

## Results and discussion

### Cloning, expression, and purification of the hsGC α subunit

The object of this study was to investigate the heme binding properties and related NO/CO binding and dissociation mechanism of the α1 subunit of hsGC. We intended to further understand the way in which the α subunit contributes to the heme binding and regulation of sGC-mediated NO singling. The first goal of this study was to obtain pure α1 subunit of hsGC using the *E. coli* efficient expression system of sGC.

The Robetta structure prediction analysis indicated that the first N-terminal 64 residues of the hsGC α1 subunit were predicted to be disordered, residues 65–248 were predicted to be an H-NOX domain, and the next 150 residues were predicted to be a Per-Arnt-Sim domain. According to the above domain prediction results, three constructs of hsGC α1 subunits—hsGCα259 (residues 65–259), hsGCα385 (residues 65–385), and hsGCα690) (residues 1–690)—were prepared. The three proteins were overexpressed as maltose binding protein fusion proteins in *E. coli*. After TEV protease cleavage, quantities of hsGCα259 with more than 90% purity (Fig. 1a), were successfully obtained. Gel filtration analysis indicated that hsGCα259 mainly existed as a homodimer, similar to that of hsGC$\beta$195 [13]. The heme-containing hsGCα259 with an $A_{Soret}/A_{280}$ ratio of about 1.5 can be acquired through heme reconstitution. Unfortunately, hsGCα385 and hsGCα690 were easily degraded and aggregated during the purification process, and thus could not be studied further. As suggested previously, the heme-binding domain of hsGC has a heme pocket and ligand binding properties similar to those of full-length hsGC [13, 15]; therefore, the following characterization focused on the heme-binding domain of sGC with hsGCα259.

### Molecular modeling of N-terminal hsGCα259

The homology model of hsGCα259, as shown in Fig. 2, was constructed on the basis of the crystal structure of the H-NOX domain of *Nostoc* sp. (Protein Data Bank entry 2O09). Although Pal and Kitagawa [11] and Hu et al. [12] suggested that the α1 H-NOX domain cavity might represent the YC-1 binding site, on the basis of upon the molecular model, there is a large cavity equivalent to the heme-binding pocket in the H-NOX domain of the $\beta$1 subunit. The heme reconstitution experiment revealed that heme can be bound in the N-terminal heme domain of hsGCα259. Therefore, we propose that the large cavity in hsGCα259 is used to accommodate the heme.

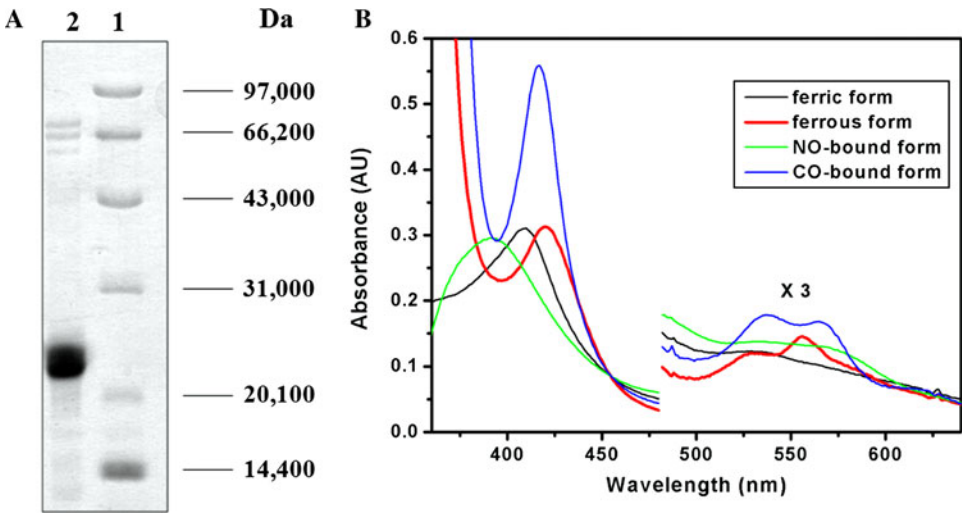


**Fig. 1** Sodium dodecyl sulfate–polyacrylamide gel electrophoresis (**a**) and electronic absorption spectra (**b**) of the N-terminus truncated human soluble guanylate cyclase α1 subunit with residues 65–259 (hsGCα259), showing the Soret peak and the α/$\beta$ region. In **a** *lane 1* marker, *lane 2* hsGCα259; in **b** the heme concentration was 3 μM in 50 mM potassium phosphate, pH 7.4, 100 mM KCl, 5% glycerol

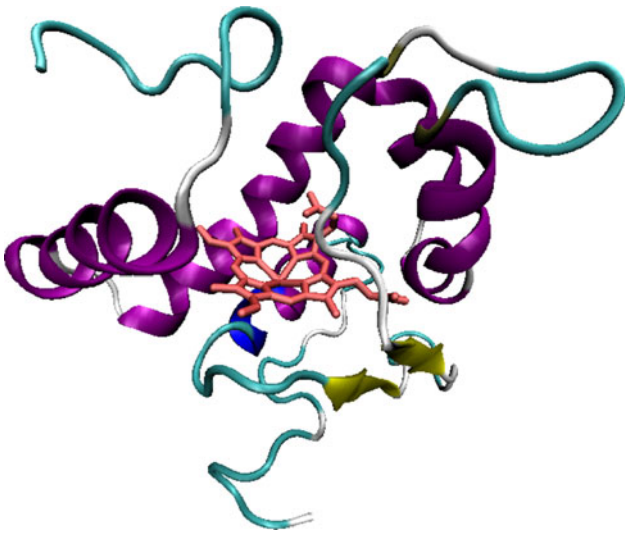

**Fig. 2** Homology model of the heme domain of hsGCα259, indicating that the large cavity of hsGCα259 is probably used to accommodate heme by noncovalent interaction

## Characterization by UV–vis spectroscopy

The electronic absorption spectra of hsGCα259 in different forms are presented in Fig. 1b, and the absorption peaks and extinction coefficients of hsGCα259 and hsGCβ195 are summarized in Table 1. All the hsGCα259 proteins exhibited spectral features similar to those of the hsGC β1 subunit [13], and the heme in the two subunits of sGC is indistinguishable; therefore, only one type of heme is observed spectrally in the sGC α1β1 heterodimer [9]. The UV–vis spectra of CO-bound and NO-bound forms indicated that the CO/NO was bound to the iron of heme and confirmed the binding of heme to hsGCα259.

**Table 1** UV–vis spectra data for N-terminus truncated human soluble guanylate cyclase α1 subunit with residues 65–259 (*hsGCα259*) and N-terminus truncated human soluble guanylate cyclase β1 subunit with residues 1-195 (*hsGCβ195*)

| Protein | Soret (ε) | β (ε) | α (ε) |
|---|---|---|---|
| hsGCα259 | | | |
| Ferric form | 408 (148) | | |
| Ferrous form | 420 (148) | 528 (19) | 555 (23) |
| NO-bound form | 393 (140) | | |
| CO-bound form | 417 (266) | 536 (28) | 562 (27) |
| hsGCβ195[a] | | | |
| Ferric form | 409 (209) | | |
| Ferrous form | 425 (189) | 533 (27) | 560 (30) |
| NO-bound form | 393 (187) | | |
| CO-bound form | 420 (193) | 535 (25) | 569 (19) |

All peak positions are in nanometers. All molecular extinction coefficients (ε) are in liters per millimole per centimeter

[a] Values from [13]

## The EPR of ferric and NO-bound hsGC

The heme-bound hsGCα259 was characterized by heme reconstitution and UV–vis spectra. Unfortunately, the difference between heme-bound hsGCα259 and hsGCβ195 cannot be distinguished via the UV–vis spectra. To address this issue, the EPR spectra of ferric and NO-bound forms of hsGCα259 and hsGCβ195 were applied, as shown in Fig. 3.

It has been proposed that His105 in the β1 subunit is the proximal heme ligand in sGC, and that the heme-binding region of sGC is localized to the N-terminus of the β1 subunit [3, 8]. The EPR spectra of the ferric hsGCα259 and hsGCβ195 were recorded as shown in Fig. 3a. hsGCβ195 shows a characteristic EPR signal absorption centered around $g \sim 4.0$, originating from the five-coordinate intermediate-spin ($S = 3/2$) ferric heme [36], which is consistent with that of the ferric β1 subunit in the five-coordinate intermediate-spin ($S = 3/2$) form with His105 as the proximal axial ligand [8, 15]. Additionally, there is another EPR signal absorption centered at $g \sim 6.0$, originating from the four-coordinate ferric heme within the protein matrix (the free heme has been removed as mentioned in "Materials and methods"). However, in the case of hsGCα259, the $g \sim 4.0$ EPR signal was absent, indicating that the axial positions of heme are vacant or occupied by weak ligands, such as $H_2O$. The multiple sequence alignment shows that the histidine is conserved throughout the H-NOX domain, with the exception of α subunits of sGC and two bacterial versions from *Rhodobacter sphaeroides* and *Magnetococcus* species. The versions lacking the conserved histidine are likely to interact with heme noncovalently [37]. Our studies demonstrated that the α1 subunit can likely bind heme via a non-covalent-interaction peptide chain at axial positions.

After NO binding to sGC, the proximal histidine dissociates from the heme iron and leads to the formation of a five-coordinate NO–heme [38–41]. Therefore, it is reasonable to predict that the NO-bound forms of hsGCα259 and hsGCβ195 have similar EPR features originating from the low-spin ($S = 1/2$) heme. The EPR spectra precisely demonstrated that both proteins share similar properties (Fig. 3b). The triplet hyperfine splitting, centered around $g \sim 2.0$, a characteristic feature of heme–nitrosyl species, indicated the binding of NO to the heme of hsGC.

## The interaction of heme with apo-hsGC

The kinetics and equilibrium constants for the interaction of heme with apo-hsGC proteins are summarized in Table 2. The absorbance time courses for the reaction of CO–heme with apo-hsGC proteins are shown in Fig. 4a. $k_{off}$ was determined from the heme transfer with

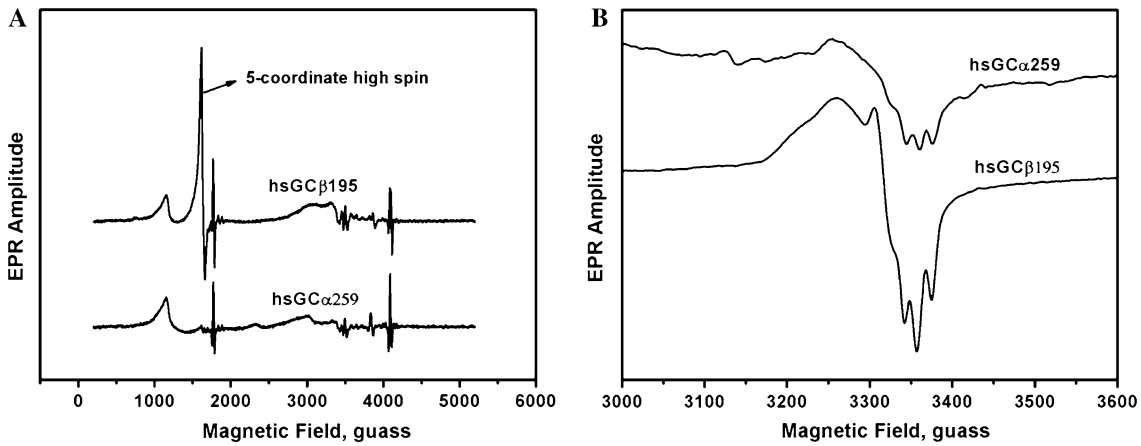


**Fig. 3** EPR spectra of the ferric and NO-bound *hsGCα259* N-terminus truncated human soluble guanylate cyclase α1 subunit with residues 65–259 and *hsGCβ195* N-terminus truncated human soluble guanylate cyclase β1 subunit with residues 1-195. **a** EPR spectra of the ferric form measured at −266 °C. **b** EPR spectra of the NO-bound form measured at −173 °C

**Table 2** Kinetics and equilibrium constants for the interaction of heme with apo forms of human soluble guanylate cyclase (hsGC) proteins

| Protein | $k_{on}$ ($\mu M^{-1}$ $s^{-1}$)[a] | $k_{off}$ ($s^{-1}$)[b] | $K_{eq}$ ($M^{-1}$)[c] |
|---|---|---|---|
| Apo-hsGCα259 | 2.6 | 0.017 | $1.52 \times 10^8$ |
| Apo-hsGCβ195 | 2.8 | 0.036 | $0.77 \times 10^8$ |
| Wild-type myoglobin[d] | 70 | $8.4 \times 10^{-7}$ | $8 \times 10^{13}$ |
| H93G myoglobin[d] | 70 | 0.012 | $6 \times 10^9$ |

[a] The association rate constants were determined from stopped-flow measurements using CO–heme in 50 mM potassium phosphate, pH 7.4, 100 mM KCl, 5% glycerol, 2 mM dithiothreitol, 30 mM $Na_2S_2O_4$

[b] Heme dissociation rates were determined from stopped-flow measurements by mixing a sixfold excess of apomyoglobin with reconstituted hsGC proteins

[c] $K_{eq}$ was calculated from the ratio $k_{on}/k_{off}$ and is an estimate of the affinity of monomeric heme for the apo-hsGC proteins

[d] Data taken from [32]

apomyoglobin and the absorbance time courses are shown in Fig. 4b.

As shown in Fig. 4a, each trace can be fitted with a double-exponential equation for two phases, which is similar to that of CO–heme with apoglobins [32, 33]. Accordingly, the faster bimolecular phase represents the combination of heme with apo-hsGC to form holo-hsGC, and the slower process represents the nonspecific binding of heme to hsGC. The association rate constant ($k_{on}$) for heme binding to globins, such as myoglobin and hemoglobin, is almost identical regardless of their structural difference, but the heme affinity difference is mainly reflected in different dissociation rates ($k_{off}$) [32, 33]. For hsGCβ195 and hsGCα259, their $k_{on}$ are almost identical, whereas $k_{off}$ of hsGCβ195 is twofold greater than that of hsGCα259. The heme dissociation of sGC is much faster than that of other hemoproteins, and this is likely the reason why heme is easily lost during purification.

Generally, the heme affinity was mainly governed by two kinds of interactions: one is the nonspecific hydrophobic interaction between the porphyrin and the apolar heme cavity, and the other is specific interaction with conserved amino acids in the heme pocket and the coordination bond between iron and the axial ligand [32]. The heme iron is bound to His105 in hsGCβ195, whereas the heme in hsGCα259 has no axial ligand. On the basis of these assumptions, we hypothesized that the heme affinity of hsGCβ195 would be higher than that of hsGCα259; however, the heme affinity of hsGCβ195, shown in Table 2, is only half of that of hsGCα259. This indicates that the Fe–His105 bond in hsGC is fragile [26], and its contribution to heme affinity is consequently small. On the other hand, the hydrophobic interactions between the porphyrin and the apolar heme cavity of hsGCα259, which was the major factor governing heme affinity [32], were probably stronger than those for hsGCβ195. The two factors mentioned above govern the heme affinity cooperatively and ultimately lead to the heme affinity of hsGCα259 being higher than that of hsGCβ195.

## Equilibrium and kinetics of CO binding to hsGC

CO binding to hsGCα259 and hsGCβ195 by CO titration was monitored spectroscopically. As shown in Fig. 5a and c, the difference spectra of hsGC obtained by CO titration display an obvious difference between hsGCα259 and hsGCβ195. There is an isosbestic point at 429 nm for hsGCβ195, indicating that six-coordinate CO-bound hsGCβ195 was formed by one-step binding without any intermediate product during the CO binding process. This property is consistent with that for sGC from *Manduca sexta* reported by Hu et al. [12]. In the case of hsGCα259, no isosbestic point was observed,

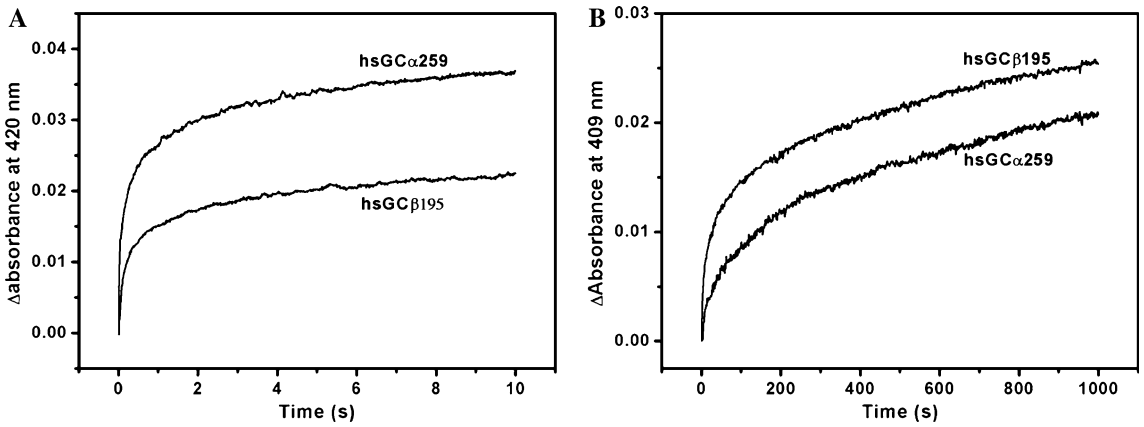


**Fig. 4** Heme binding and dissociation of hsGCα259 and hsGC$\beta$195 monitored by stopped-flow measurements at 25 °C. **a** Time courses for CO–heme binding to hsGCα259 and hsGC$\beta$195. The reaction was initiated by mixing 1 μM apo-human soluble guanylate cyclase (sGC) with CO–heme solution and was monitored at 420 nm. The time courses were then fitted to a double-exponential expression. **b** Time courses for heme transfer from hsGCα259 and hsGC$\beta$195 to apomyoglobin. Heme dissociation rate constants ($k_{off}$) were measured using a stopped-flow apparatus or UV–vis spectrometer with kinetic mode in heme transfer experiments using the apomyoglobin assay. The heme transfer process was monitored at 409 nm

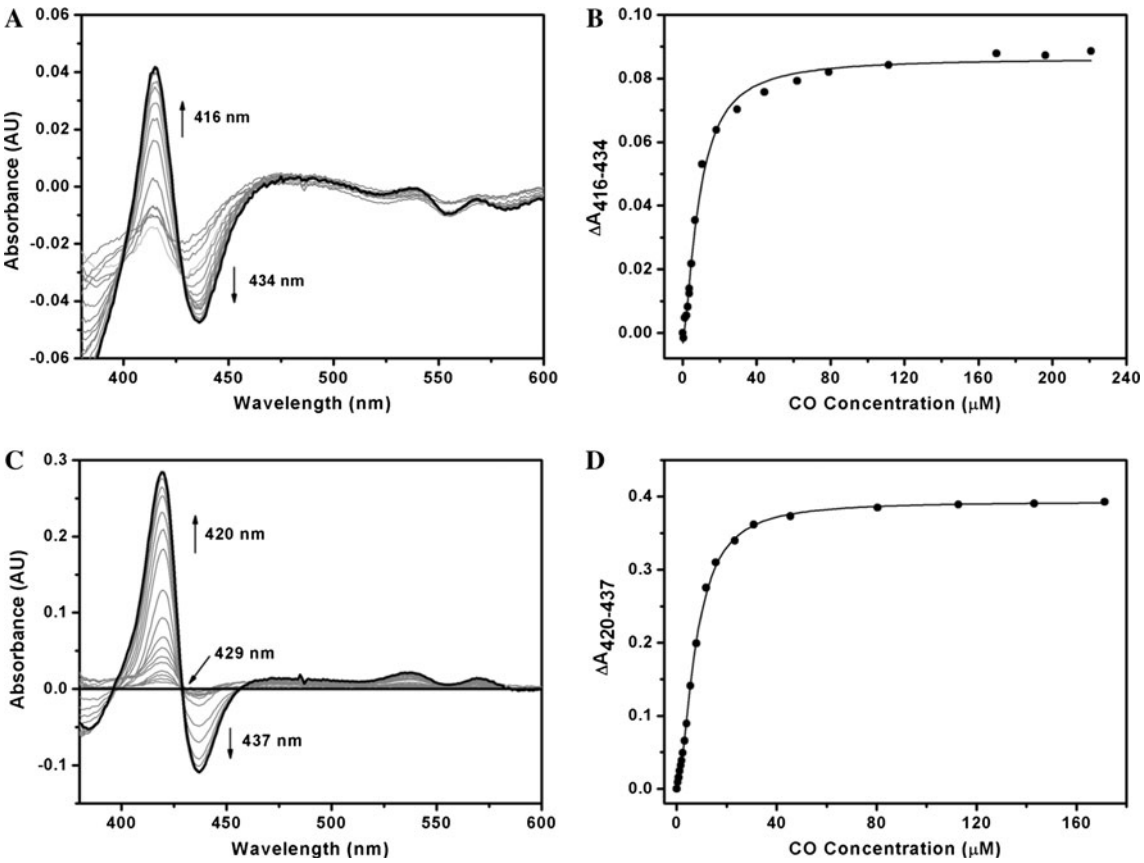


**Fig. 5** CO titration equilibrium study of hsGCα259 and hsGC$\beta$195 at 20 °C. Difference spectra of hsGCα259 (**a**) and hsGC$\beta$195 (**c**) during the CO titration process, and the fitting of the difference spectra by a single-site CO-saturation model to obtain the measured CO dissociation constants ($K_d$): **b** fitting curve for hsGCα259; **d** fitting curve for hsGC$\beta$195

suggesting that at least one intermediate product was formed accompanied by CO binding. Combined with the finding from the EPR spectra that there is no strong axial ligand for the heme of hsGCα259, there is a possibility that CO can bind to both the proximal and the distal axial positions of the heme of hsGCα259.

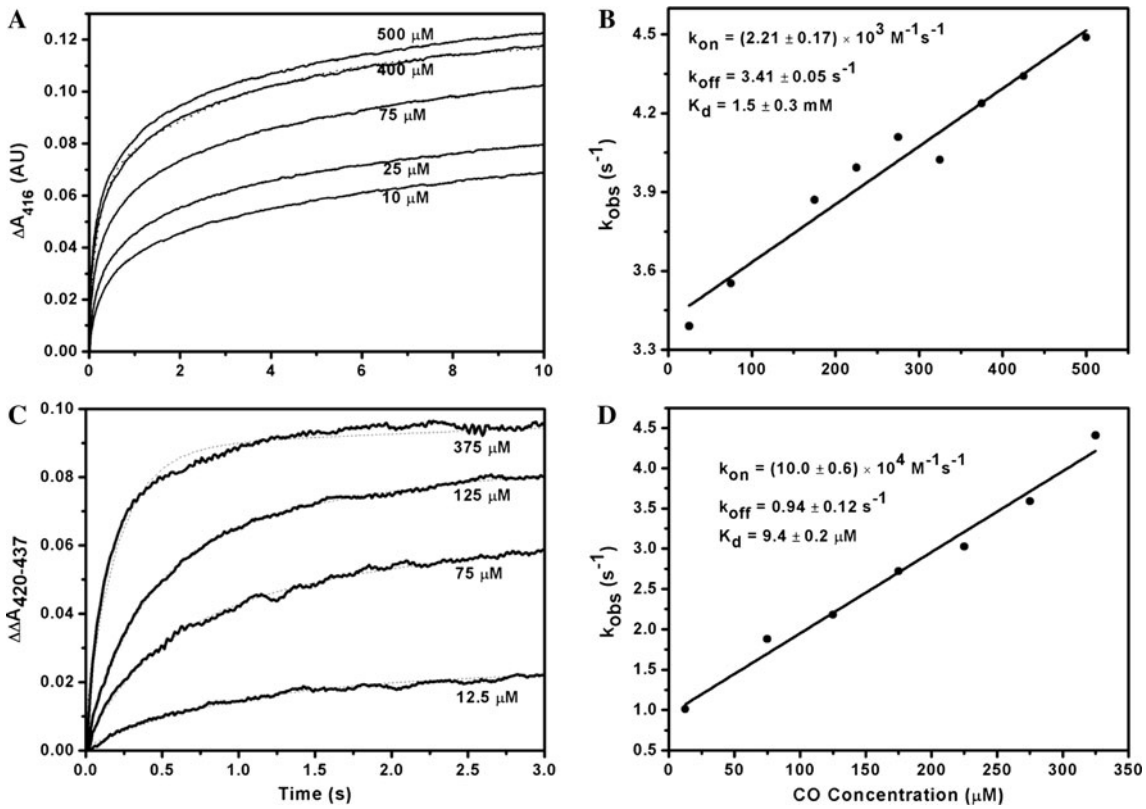


**Fig. 6** CO binding kinetics of hsGC$\alpha$259 and hsGC$\beta$195 at 25 °C measured by the stopped-flow method. The time courses of CO binding to hsGC$\alpha$259 (**a**) and hsGC$\beta$195 (**c**) in the presence of a series of concentration of CO (original data *solid line*, single-exponential fitting curve *dashed line*). The concentrations shown are the final concentrations after mixing. Plots of $k_{obs}$ against CO concentration for hsGC$\alpha$259 (**b**) and hsGC$\beta$195 (**d**). $k_{on}$ and $k_{off}$ were obtained from the slope and intercept, respectively. $K_d$ was calculated by $k_{off}/k_{on}$

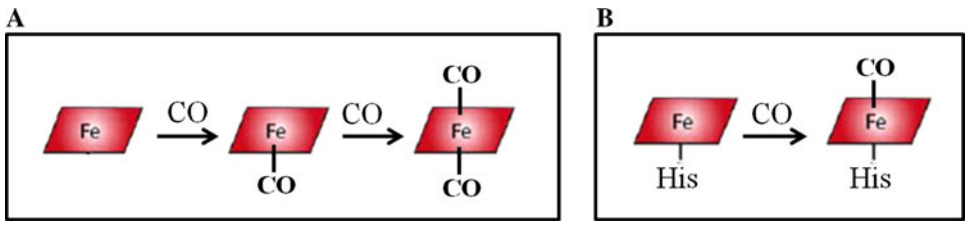


**Fig. 7** Possible CO binding model for sGC. **a** CO binding to the heme of hsGC$\alpha$259; in this case, CO can possibly bind to the $Fe^{2+}$ of heme from the axial position. **b** CO binding to the heme of hsGC$\beta$195; $\beta$1His105 is ligated to the heme in the ferrous form, and CO binds to the distal ligand position to form the six-coordinate form by simple one-step binding

$K_d$ for CO binding to hsGC was obtained by two-independent methods (Figs. 5, 6). For hsGC$\beta$195, the calculated $K_d$ ($k_{off}/k_{on}$) was in good agreement with the value obtained from CO titration equilibrium, indicating that the six-coordinate CO-bound hsGC$\beta$195 was formed by one-step binding of CO to the five-coordinate heme, as reported previously [22, 42]. However, the calculated $K_d$ (1,500 μM) for hsGC$\alpha$259 was 200-fold larger than that obtained from equilibrium measurement (7 μM), suggesting that a simple one-step binding model cannot describe the binding of CO to hsGC$\alpha$259. A more complicated model is required to describe the CO binding process. On the basis of these results, a possible CO binding model of hsGC is proposed in Fig. 7.

Stone and Marletta [42] demonstrated that the heme of sGC has a low CO affinity, due primarily to fast CO off rates, by comparing the equilibrium and kinetic constants of sGC with those of other hemoproteins, such as hemoglobin, myoglobin, and FixL. Interestingly, the kinetics of CO binding to eukaryotic sGC and prokaryotic sGC (Table 3) indicated that the difference of CO affinity is due to the variation of $k_{on}$. Additionally, the measured dissociation constant ($K_d$) of each subunit was only 10% of that in sGC heterodimer, indicating that CO affinity was further

**Table 3** Kinetic and equilibrium constants of CO binding of soluble guanylate cyclase (sGC)

| Protein | $k_{off}$ ($s^{-1}$) | $k_{on}$ ($M^{-1}$ $s^{-1}$) | $K_d$ (calculated, μM) | $K_d$ (measured, μM) |
|---|---|---|---|---|
| hsGCα259 | 3.41 ± 0.05 | (2.21 ± 0.17) × $10^3$ | 1,500 ± 300 | 6.9 ± 0.2 |
| hsGCβ195 | 0.94 ± 0.12 | (1.00 ± 0.06) × $10^5$ | 9.4 ± 0.2 | 7.6 ± 0.2 |
| Bovine sGC[a] | 3.5 ± 0.5 | (3.58 ± 0.15) × $10^4$ | 98 ± 15 | 97 ± 9 |
| *Manduca sexta* sGC | 2.01 ± 0.05 | (2.84 ± 0.07) × $10^4$ | 71 | 77 ± 7 |
| *Nostoc* sp. H-NOX | 3.6 | 3 × $10^6$ | 1.4 | 1.2 |

$K_d$ (calculated) and $K_d$ (measured) are the values calculated from CO kinetics and measured from CO titration, respectively

*H-NOX* heme–nitric oxide/oxygen binding domain

[a] Data adapted from [12, 22, 43]

regulated by the heterodimerization of two subunits. The domain–domain interaction of sGC might have an influence on the CO affinity of the full-length hsGC α1 and β1 subunits.

### Kinetics of NO dissociation from hsGC

The difference spectra of NO dissociation from hsGC and the corresponding plots of NO dissociation are shown in Fig. 8. The observed rate constants and fractional amplitudes for NO dissociation are summarized in Table 4. The plots of NO dissociation were best fitted with a double-exponential equation, and not a single-exponential equation as reported in [35]. This result suggested that the NO dissociation from sGC was complex with at least two release phases, which coincides with that with rat, bovine and *M. sexta* sGC [23, 43, 44]. It was proposed that the NO-bound sGC is a mixture of two different five-coordinate species with open and closed conformations, respectively [23].

From Table 4, the parameters of NO dissociation from hsGCβ195 were nearly identical to those from rat β1 (1–194) reported previously [23]. When compared with hsGCβ195, hsGCα259 has a smaller $k_1$ (the faster rate) but a larger $k_2$ (the slower rate), and more obviously the population of sGC with a faster dissociation rate increased. This suggested that the heme–nitrosyl complexes of hsGCα259 and hsGCβ195 adopted different conformations or different compositions of the mixed conformations of five-coordinate species.

$k_1$ of rat sGC heterodimer is fourfold larger than that of rat β1 (1–194). Thus, we propose that the N-terminal heme domains of the α1 and β1 subunits will interact with each other and correspondingly influence the NO dissociation from sGC. We attempted to reconstitute the α1β1 heterodimer of the heme domain in vitro to examine this possibility, but unfortunately the heterodimer was not formed. The homodimerization of each subunit could inhibit the formation of the α1β1 heterodimer of heme domain. The sGC heterodimerization might be a regulated process in living cells [45]. Furthermore, the NO dissociation from *M. sexta* sGC was about 10 times faster than that from rat sGC, represented in Table 4, suggesting that NO affinity might be increased upon decreasing the NO dissociation rate to better fulfill $NO/O_2$ ligand discrimination from an evolutionary aspect.

### The role of YC-1

There is a large cavity in the homology model of hsGCα259 (Fig. 2) and the role of the cavity is unknown. Recently, YC-1 was proposed to occupy the cavity of the sGC α1 subunit and the docking model was described [11]; however, there is no direct evidence for this hypothesis. YC-1 can synergistically activate sGC with CO and NO; however, the mechanism of activation and the binding site for YC-1 are still a matter of debate [11, 12, 22, 23, 46, 47]. In this study, the effect of YC-1 on CO binding to hsGCα259 and hsGCβ195 was explored (Fig. 9). The difference spectra for CO binding in the presence and absence of YC-1 were fitted to a single-site saturation model, from which there is no obvious change in CO affinity after the addition of 50 μM YC-1. This result is similar to that reported by Stone and Marletta [22].

The result of isothermal titration calorimetry for the reaction of YC-1 with apo-hsGCα259 (Fig. 10) indicated that there is no obvious (or very weak) interaction between YC-1 and apo-hsGCα259. The cavity likely accommodates heme as represented in the homology model (Fig. 2). The physiological sGC is a heterodimer composed of α and β subunits, and both the subunits contribute to the heme binding, whereas YC-1 is thought to be a heme-dependent activator of sGC [3]. Therefore, YC-1 may have different effects on the heterodimeric sGC from those on the homodimer of a single subunit. The heterodimeric mechanism of sGC remains ambiguous [45, 48–50], and further study of the activation mechanism of sGC by YC-1 is required.

## Conclusion

In summary, the recombinant hsGC α1 subunit was expressed in *E. coli* and purified for the first time. The

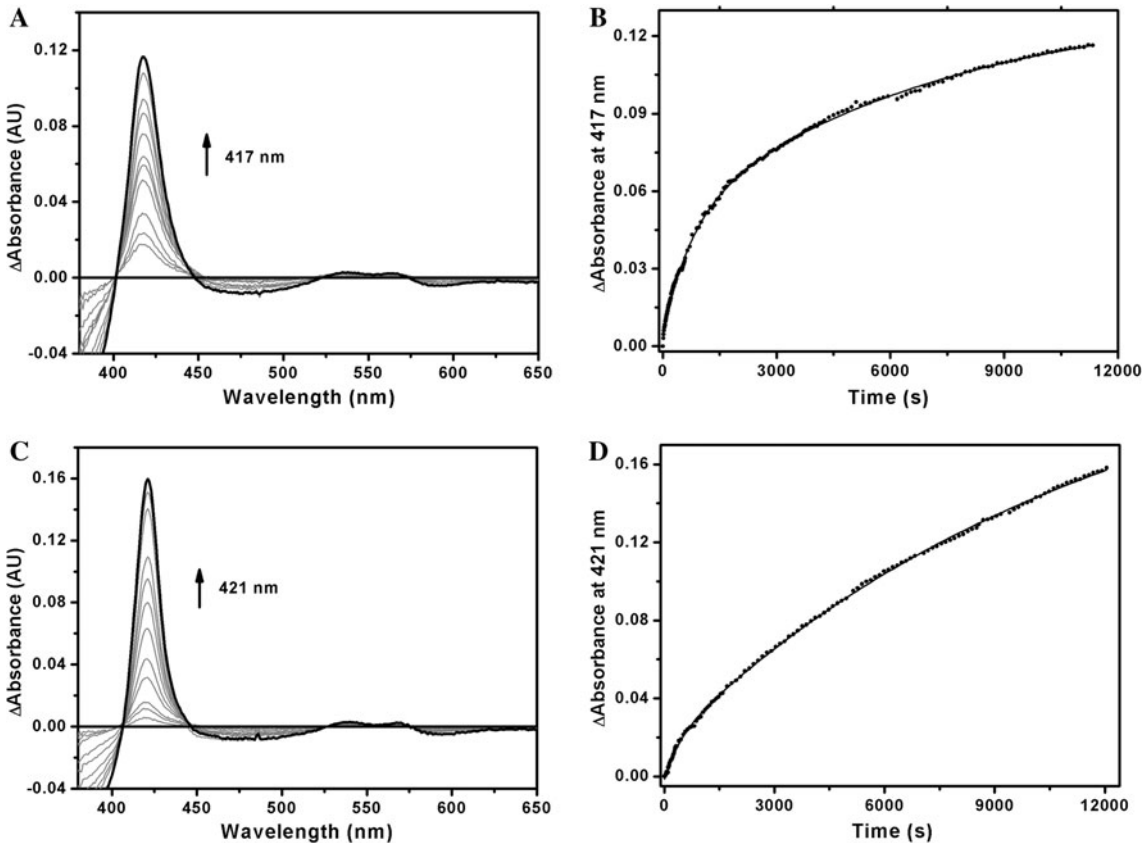


**Fig. 8** Difference spectra and absorbance time courses for observed NO dissociation from the heme domain of human sGC with the CO/dithionite trapping method at 25 °C. Difference spectra of hsGC$\alpha$259 (**a**) and hsGC$\beta$195 (**c**) during the NO dissociation, and the time courses for hsGC$\alpha$259 (**b**) and hsGC$\beta$195 (**d**) during the NO dissociation

**Table 4** Observed rate constants and fractional amplitudes for NO dissociation from hsGC and sGC from other species

| Protein | $k_1$ ($s^{-1}$) | $k_2$ ($s^{-1}$) | $\Delta A_1/\Delta A_2$ (%) |
|---|---|---|---|
| hsGC$\alpha$259 | $(1.32 \pm 0.05) \times 10^{-3}$ | $(1.40 \pm 0.08) \times 10^{-4}$ | 33:67 |
| hsGC$\beta$195 | $(2.51 \pm 0.17) \times 10^{-3}$ | $(0.85 \pm 0.02) \times 10^{-4}$ | 7:93 |
| Rat sGC[a] | $(11.8 \pm 7.1) \times 10^{-3}$ | $(1.2 \pm 0.2) \times 10^{-4}$ | 5:95 |
| Rat $\beta$1 (1–194)[a] | $(3.0 \pm 0.2) \times 10^{-3}$ | $(1.3 \pm 0.1) \times 10^{-4}$ | 6:94 |
| *Manduca sexta* sGC[b] | $(101 \pm 8) \times 10^{-3}$ | $(66 \pm 8) \times 10^{-4}$ | 56:44 |

Values are averages of three dissociation experiments at 20 °C

[a] Data at 10 °C from [23]

[b] Data at 20 °C from [12]

heme binding and related NO/CO binding kinetics of both subunits were investigated via heme reconstitution, UV–vis spectroscopy, EPR spectroscopy, stopped-flow kinetics, and homology modeling. These results indicated that the $\alpha$1 subunit of hsGC, lacking the conserved axial ligand, is likely to interact with heme noncovalently although the molecular mechanism of heme binding with the heterodimeric sGC is still intangible. On the basis of the equilibrium and kinetics of CO binding to sGC, one possible CO binding model was proposed. CO binds to hsGC$\beta$195 by simple one-step binding, whereas CO binds to hsGC$\alpha$259 possibly from both axial positions through a more complex process. The kinetics of NO dissociation from hsGC indicated that the NO dissociation from sGC was complex, with at least two release phases, and hsGC$\alpha$259 has a smaller $k_1$ (the faster rate) but a larger $k_2$ (the slower rate). However, further study is required to understand the mechanism by which the N-terminal heme domains of the $\alpha$1 and $\beta$1 subunits interact with each other and correspondingly influence NO dissociation from

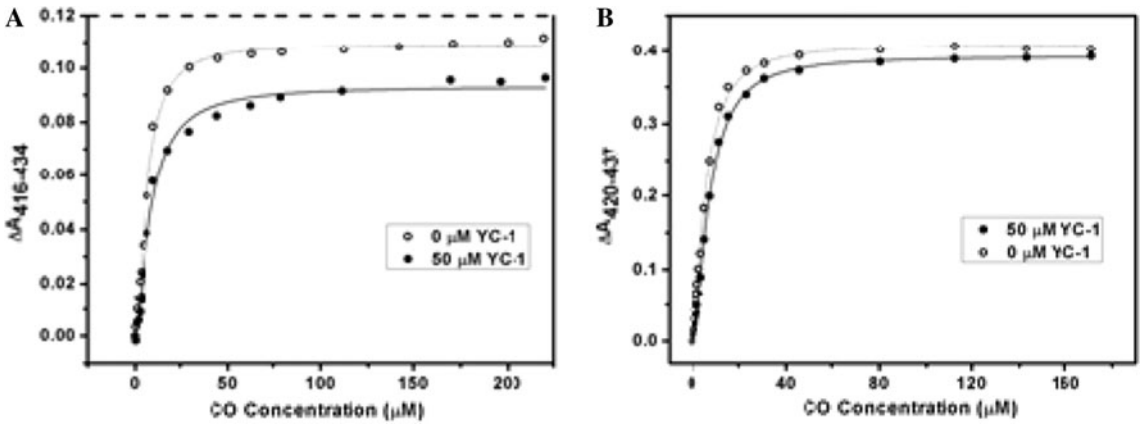


**Fig. 9** Effect of 5-[1-(phenylmethyl)-1*H*-indazol-3-yl]-2-furanmethanol (*YC-1*) on CO binding to hsGC$\alpha$259 (**a**) and hsGC$\beta$195 (**b**). The difference spectra for CO binding in the presence and absence of YC-1 were fitted to a single-site saturation model

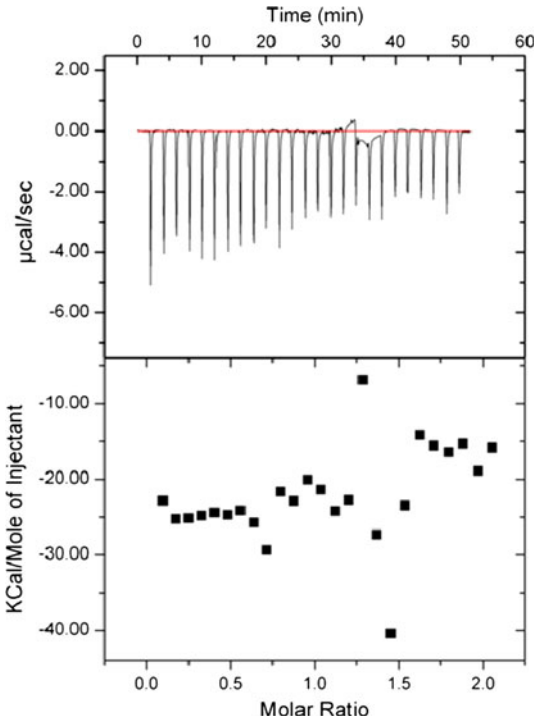


**Fig. 10** Calorimetric isothermal titration for the reaction of YC-1 with apo-hsGC$\alpha$259 at 25 °C. *Top*: Raw data for 252-μl injections of 1 mM YC-1 into 20 μM apo-hsGC$\alpha$259 contained in the cell (cell volume 200 μl), with intervals of 2 min between injections. The reaction buffer was 50 mM 4-(2-hydroxyethyl)-1-piperazineethane sulfonic acid, pH 7.4, 1 mM tris(2-carboxyethyl)phosphine, 100 mM NaCl. *Bottom*: Integrated curve showing the experimental points that were obtained by integration of the peaks in the plot above plotted against the molar ratio of the YC-1 to apo-hsGC$\alpha$259 in the reaction cell. Curve fitting was performed using Omega

sGC. Additionally, the role of the cavity of the $\alpha$1 subunit of hsGC was explored, and the results indicate that the cavity likely accommodates heme, as shown in the homology model (Fig. 2). These results are beneficial for understanding the overall structure of the heme binding site of hsGC and the NO/CO signaling mechanism.

**Acknowledgments** The authors would thank Jiangfeng Du for his support of EPR measurements. This work was financially supported partly by Shanghai Pujiang Talent Project (08PJ14017), National Natural Science Foundation of China (no. 20771029, no. 91013001, no. 31070211), Shanghai Leading Academic Discipline Project (B108), and the PhD program of the Education Ministry of China (20100071110011), to X.T.

## References

1. Chen KJ, Pittman RN, Popel AS (2008) Antioxid Redox Signal 10:1185–1198
2. Denninger JW, Marletta MA (1999) Biochim Biophys Acta 1411:334–350
3. Evgenov OV, Pacher P, Schmidt PM, Hasko G, Schmidt HH, Stasch JP (2006) Nat Rev Drug Discov 5:755–768
4. Wang-Rosenke Y, Neumayer HH, Peters H (2008) Curr Med Chem 15:1396–1406
5. Pellicena P, Karow DS, Boon EM, Marletta MA, Kuriyan J (2004) Proc Natl Acad Sci USA 101:12854–12859
6. Schmidt PM, Schramm M, Schroder H, Wunder F, Stasch JP (2004) J Biol Chem 279:3025–3032
7. Stone JR, Marletta MA (1994) Biochemistry (Mosc) 33:5636–5640
8. Foerster J, Harteneck C, Malkewitz J, Schultz G, Koesling D (1996) Eur J Biochem 240:380–386
9. Stone JR, Marletta MA (1995) Biochemistry (Mosc) 34:14668–14674
10. Tomita T, Tsuyama S, Imai Y, Kitagawa T (1997) J Biochem 122:531–536
11. Pal B, Kitagawa T (2010) Biochem Biophys Res Commun 397:375–379
12. Hu X, Murata LB, Weichsel A, Brailey JL, Roberts SA, Nighorn A, Montfort WR (2008) J Biol Chem 283:20968–20977
13. Zhong F, Wang H, Ying T, Huang ZX, Tan X (2010) Amino Acids 39:399–408
14. Lee YC, Martin E, Murad F (2000) Proc Natl Acad Sci USA 97:10763–10768
15. Karow DS, Pan DH, Davis JH, Behrends S, Mathies RA, Marletta MA (2005) Biochemistry (Mosc) 44:16266–16274

16. Burstyn JN, Yu AE, Dierks EA, Hawkins BK, Dawson JH (1995) Biochemistry (Mosc) 34:5896–5903
17. Friebe A, Schultz G, Koesling D (1996) EMBO J 15:6863–6868
18. Denninger JW, Schelvis JPM, Brandish PE, Zhao Y, Babcock GT, Marletta MA (2000) Biochemistry (Mosc) 39:4191–4198
19. Ibrahim M, Derbyshire ER, Marletta MA, Spiro TG (2010) Biochemistry (Mosc) 49:3815–3823
20. Koglin M, Behrends S (2003) J Biol Chem 278:12590–12597
21. Li Z, Pal B, Takenaka S, Tsuyama S, Kitagawa T (2005) Biochemistry (Mosc) 44:939–946
22. Stone JR, Marletta MA (1998) Chem Biol 5:255–261
23. Winger JA, Derbyshire ER, Marletta MA (2007) J Biol Chem 282:897–907
24. Berry EA, Trumpower BL (1987) Anal Biochem 161:1–15
25. Chivian D, Kim DE, Malmstrom L, Bradley P, Robertson T, Murphy P, Strauss CE, Bonneau R, Rohl CA, Baker D (2003) Proteins 53(Suppl 6):524–533
26. Poulos TL (2006) Curr Opin Struct Biol 16:736–743
27. Ma X, Sayed N, Beuve A, van den Akker F (2007) EMBO J 26:578–588
28. Autenrieth F, Tajkhorshid E, Baudry J, Luthey-Schulten Z (2004) J Comput Chem 25:1613–1622
29. Laidig KE, Daggett V (1996) Fold Des 1:335–346
30. Mackerell AD Jr, Feig M, Brooks CL 3rd (2004) J Comput Chem 25:1400–1415
31. Guryev OL, Gilep AA, Usanov SA, Estabrook RW (2001) Biochemistry (Mosc) 40:5018–5031
32. Hargrove MS, Barrick D, Olson JS (1996) Biochemistry (Mosc) 35:11293–11299
33. Hargrove MS, Singleton EW, Quillin ML, Ortiz LA, Phillips GN Jr, Olson JS, Mathews AJ (1994) J Biol Chem 269:4207–4214
34. Lamar GN, Toi H, Krishnamoorthi R (1984) J Am Chem Soc 106:6395–6401
35. Kharitonov VG, Sharma VS, Magde D, Koesling D (1997) Biochemistry (Mosc) 36:6814–6818
36. Walker FA (2003) Inorg Chem 42:4526–4544
37. Iyer LM, Anantharaman V, Aravind L (2003) BMC Genomics 4:5
38. Makino R, Matsuda H, Obayashi E, Shiro Y, Iizuka T, Hori H (1999) J Biol Chem 274:7714–7723
39. Nioche P, Berka V, Vipond J, Minton N, Tsai AL, Raman CS (2004) Science 306:1550–1553
40. Stone JR, Sands RH, Dunham WR, Marletta MA (1995) Biochem Biophys Res Commun 207:572–577
41. Yazawa S, Tsuchiya H, Hori H, Makino R (2006) J Biol Chem 281:21763–21770
42. Stone JR, Marletta MA (1995) Biochemistry (Mosc) 34:16397–16403
43. Tsai AL, Berka V, Martin F, Ma X, van den Akker F, Fabian M, Olson JS (2010) Biochemistry (Mosc) 49:6587–6599
44. Kharitonov VG, Russwurm M, Magde D, Sharma VS, Koesling D (1997) Biochem Biophys Res Commun 239:284–286
45. Zabel U, Hausler C, Weeger M, Schmidt HH (1999) J Biol Chem 274:18149–18152
46. Kharitonov VG, Sharma VS, Magde D, Koesling D (1999) Biochemistry (Mosc) 38:10699–10706
47. Sharma VS, Magde D, Kharitonov VG, Koesling D (1999) Biochem Biophys Res Commun 254:188–191
48. Ma X, Sayed N, Baskaran P, Beuve A, van den Akker F (2008) J Biol Chem 283:1167–1178
49. Wagner C, Russwurm M, Jager R, Friebe A, Koesling D (2005) J Biol Chem 280:17687–17693
50. Zhou Z, Gross S, Roussos C, Meurer S, Muller-Esterl W, Papapetropoulos A (2004) J Biol Chem 279:24935–24943